Natural convection heat and mass transfer in a micropolar fluid-saturated non-Darcy porous regime with Radiation and thermophoresis effects

A.Y. Bakier
Department of Mathematics, Assiut University, Assiut, Egypt
Department of Mathematics,
Assiut University,
Assiut, Egypt,
Email:*ahmedy.bakier@gmail.com*; *aybakier@yahoo.com*

Abstract

An analysis is presented for the steady thermal convection heat and mass transfer in a micropolar-fluid-saturated non-Darcian porous medium in the presence of radiation and thermophoresis effects. The governing boundary layer equations for momentum, energy, species transfer and angular momentum (micro-rotation) are transformed from an (x, y)*, coordinate system into* (η)*, coordinate system. The influence of Darcy number* (D_a)*, Forchheimmer number* (F_s)*, local Grashof number* (G_r)*, Prandtl number* (P_r)*, Schmidt number* (S_c)*, radiation* (R) *and thermophoresis* (κ)*, surface parameter* (s)*, on the velocity, temperature, concentration profiles and angular velocity (micro-rotation) are studied graphically. Applications for the problem arise in chemical engineering systems and geothermal energy systems.*

Key words: Convection , porous media, thermophoresis, radiation, micropolar fluid, heat and mass transfer.

Introduction

Micropolar fluids are a subset of the micromorphic fluid theory introduced in a pioneering paper by Eringen in [1]. They constitute an important branch of non-Newtonian fluid dynamics where microrotation effects as well as microinertia are exhibited. Such fluids have been shown to accurately simulate the flow characteristics of polymeric additives, geomorphological sediments, colloidal suspensions, haematological suspensions, liquid crystals, lubricants etc. In the context of chemical engineering, aerospace engineering and also industrial manufacturing processes, heat and mass transfer in micropolar fluids is also important. Ramachandran and Mathur [2] investigated the heat transfer in the stagnation point flow of a micropolar fluid. Vidyanidhi and Murty [3] examined the dispersion of a chemically non-reacting and chemically reacting solute in a micropolar fluid, for a circular pipe geometry. Soundalgekar and Takhar [4] analyzed numerically the micropolar thermo-convection

past a wedge, showing that micropolarity reduces drag (skin friction) and also heat transfer rates. Viscous dissipation effects in micropolar thermo-fluid dynamics have also attracted some attention. Important studies in this regard were reported by Migun and Prokhorenko [5] who studied the Couette channel convection flow of a micropolar liquid with viscous energy dissipation. The effects of viscous heating on micropolar lubrication flows was considered by Khonsari and Brewe [6] who demonstrated that the heat generation due to viscous dissipation exerts a marked effect on the load-carrying of a journal bearing lubricated with micropolar fluid. Hassanien et al. [7] analyzed the natural convection in micropolar boundary layer flow. Hassanien and Al-arabi [8] they studied unsteady mixed convection boundary layer flow near the stagnation point on a heated vertical plate embedded in a fluid saturated porous medium. Ching [9] extend the work of Nazar et al. [10] further to analyze the heat and mass transfer by natural convection along a sphere with constant wall temperature and concentration in a microplar fluid. Thermophoresis particle deposition in a non-Darcy porous medium under the influence of Soret, Dufour effects by Partha[11].

An excellent summary of Darcian convection heat transfer flows and also certain non-Darcian Newtonian flows is available in the monograph by Ingham and Pop [12]. The so-called Darcy-Brinkman model for boundary vorticity has been examined by Vafai and Tien [13] and later by Bég et al [14], the latter study also incorporating the influence of Eckert number on the heat transfer in a porous medium. Bég et al[15] study the Darcy– Forchheimer porous drag force model to study thermal convection from a continuously moving surface immersed in a Newtonian fluid-saturated porous medium. Inertial effects on porous media transport have been generally studied using the Darcy-Forchheimer model which uses a quadratic impedance term for inertial drag. Micropolar transport in porous media has also received some consideration in the literature, owing to applications in polymeric filtration dynamics. Takhar et al[16] study finite element biomagnetic hydrodynamics in a two dimensional non-Darcian porous medium.

Thermophoresis is a phenomenon by which submicron sized particles suspended in a non-isothermal gas acquire a velocity relative to the gas in the direction of decreasing temperature. The velocity acquired by the particles is called thermophoretic velocity and the force experienced by the suspended particles due to the temperature gradient is known as thermophoretic force. Recently, Chamkha and Pop [17] studied the effect of thermophoretic particle deposition in free convection boundary layer from a vertical flat plate embedded in a porous medium. Bakier and Mansour [18] deals with heat and mass transfer by steady laminar boundary layer flow of Newtonian, viscous fluid over a vertical flat plate embedded in a fluid-saturated porous medium in the presence of thermophoretic and magnetic field. Motivated by the above investigations and possible applications, it is interest in the present work to study combination of Thermophoresis, radiation effects, Darcian resistance, Forchheimer quadratic (inertial) drag, buoyancy, micropolarity and surface mass flux on the coupled heat and mass transfer of a micropolar liquid in a Darcy- Forchheimer saturated porous medium [figure 1]. The study has applications in chromatography, polymeric filtration, electronic fabrication and geophysical transport.

Analysis

We consider the coupled convective heat and mass transfer of a viscous, incompressible, non-conducting, micropolar fluid through a non-Darcy, isotropic,

homogenous porous medium. The x-axis is directed along the vertical surface and the y-axis is transverse to this. Both the vertical surface and the fluid are maintained initially at the same temperature and concentration. Incorporating viscous heating effects, wall mass flux and buoyancy, under the Boussinesq approximation, the boundary layer equations may be presented as follows:

The governing conservation equations for the flow regime can be shown to be as follows:

$$\frac{\partial u}{\partial x}+\frac{\partial v}{\partial y}=0 \qquad (1)$$

$$u\frac{\partial u}{\partial x}+v\frac{\partial v}{\partial y}=\nu\frac{\partial^2 u}{\partial y^2}+k_1\frac{\partial N}{\partial y}+g\beta_t(T-T_\infty)+g\beta_c(C-C_\infty)-\frac{\nu}{K}u-\frac{b}{K}u^2$$

(2)

$$u\frac{\partial T}{\partial x}+v\frac{\partial T}{\partial y}=\alpha\frac{\partial^2 T}{\partial y^2}-\frac{1}{\rho c_p}\frac{\partial q_r}{\partial y} \qquad (3)$$

$$u\frac{\partial C}{\partial x}+v\frac{\partial C}{\partial y}=D\frac{\partial^2 C}{\partial y^2}-\frac{\partial}{\partial y}(V_T C) \qquad (4)$$

$$u\frac{\partial N}{\partial x}+v\frac{\partial N}{\partial y}=\frac{\gamma}{\rho j}\frac{\partial^2 N}{\partial y^2}-\frac{k}{\rho j}\left(2N+\frac{\partial u}{\partial y}\right) \qquad (5)$$

Where, the quantity q_r on the right hand side of Eq. (3) represents the radiative heat flux in the $y-directions$. The radiative heat flux term is simplified by the Rosseland approximation as follows[see [19]]:

$$q_r=-\frac{4\sigma_0}{3k^*}\frac{\partial T^4}{\partial y} \qquad (6)$$

where σ_0 is the Stefan–Boltzmann constant and k^* is the mean absorption coefficient.

We now expand T^4 in a Taylor series about T_∞ as follows:

$$T^4=T_\infty^4+4T_\infty^3(T-T_\infty)+6T_\infty^2(T-T_\infty)^2+-----$$

Neglecting higher-order terms in the above equation beyond the first degree in $(T-T_\infty)$, we get

$$T^4\cong -3T_\infty^4+4T_\infty^3T$$

As a consequence, the thermophoretic velocity V_T, which appears in Eq. (4), may be expressed in the following form[see [20]]:

$$V_T=-\frac{\kappa\nu}{T}\frac{\partial T}{\partial y} \qquad (7)$$

The corresponding boundary conditions on the vertical surface and in the free stream can be defined now as follows:

$$\text{at} \quad y=0: \quad u=U_0,\ v=V_0(x), \qquad T=T_w \quad C=C_w,\ N=-s\left(\frac{\partial u}{\partial y}\right) \tag{8}$$

$$as \quad y\to\infty: \quad u\to 0, \quad v\to 0, \qquad T\to T_\infty, \quad C\to C_\infty, \quad N\to 0$$

Where, $V_0(x)$ transpiration (lateral mass flux) velocity at the wall (vertical surface), K is permeability of porous medium (hydraulic conductivity), b is Forchheimer constant (geometrical). We note that $V_o<0$ represents suction (removal of micropolar fluid from the regime via the perforated wall) while $V_o>0$ represents mass injection (blowing) into the flow regime.

To simplify a numerical solution, while still retaining the essential physics of the flow regime, we introduce a set of pseudo-similarity transformations, viz:

$$\eta = y\sqrt{\frac{U_o}{2\nu x}}, \quad \psi=\sqrt{2\nu x U_0}\,f\ ,\ \theta=\frac{T-T_\infty}{T_W-T_\infty}, \phi=\frac{C-C_\infty}{C_W-C_\infty}\ ,$$

$$N=-\sqrt{\frac{U_o}{2\nu x}}U_o\,h\ , \tag{9}$$

where η is dimensionless transverse coordinate, f is dimensionless stream function, θ is dimensionless temperature function, ϕ is dimenionless concentration function, h is dimensionless micro-rotation (angular velocity), $\Delta T=T_w+T_\infty,\ \Delta C=C_w+C_\infty$. The conservation equations are now transformed to the following system of coupled, non-linear ordinary differential equations, in terms of f, f', θ, ϕ, h viz:

The transformed governing equations for bonundary layer flows become:

$$\begin{aligned}
&f'''+Bh'+ff''+G_r\theta+G_m\phi-\frac{1}{D_aR_e}f'-\frac{F_S}{D_a}f'^2=0\\
&\theta''\left(1+\tfrac{4}{3}R\right)+P_r f\theta'=0\\
&\phi''+S_c f\phi'+\frac{\kappa S_c}{(\theta+c_T)}\left[\theta''\phi+\theta'\phi'-\frac{\theta'^2\phi}{(\theta+c_T)}\right]=0\\
&\lambda h''-2\frac{\lambda}{GG}(2h+f'')+f'h+fh'=0
\end{aligned} \tag{10}$$

where $\theta=\frac{T-T_\infty}{T_w-T_\infty}$, $\phi=\frac{C-C_\infty}{C_w-C_\infty}$, $R_e=\frac{U_0L^2}{2\nu x}$ is the local Reynolds number, $G_r=4g\beta_t(T_w-T_\infty)\nu/u_\infty^3$ is the local Grashof number, $G_m=4g\beta_c(C_w-C_\infty)\nu/u_\infty^3$ is the local modified Grashof number, $P_r=\frac{\alpha}{\nu}$, is the Prandtl number, $S_c=\frac{\nu}{D}$ is the Schmidt number, $\lambda=\frac{\gamma}{\rho j\nu}$ and $GG=\frac{\gamma U_0}{\nu x k}$ are micropolar parameters(dimensionless

material properties), $D_a = \frac{K}{L^2}$ is the Darcy number, $F_s = \frac{2bx}{L^2}$ is the Forchheimer Number, $B = \frac{k_1}{\nu}$ and $k_1 = \frac{k}{\rho}(k_1 \succ 0)$ are the Coupling constant parameters.

The transformed boundary conditions are given by :

$$\text{at } \eta = 0: f = -V_o\sqrt{\frac{2x}{\nu U_o}}, f' = 1, \quad \theta = 1, \quad \phi = 1, \quad h = -sf''(0)$$

$$as \quad \eta \to \infty: f' \to 1, \quad \theta \to 0, \quad \phi \to 0, \quad h \to 0$$

(11)

Where a prime denotes ordinary differentiation with respect to η.

Results and Discussion

The system of ordinary differential equations (10) along with the boundary conditions (11), are integrated numerically by means of the fourth-order Runge-Kutta method, with shooting technique. In order to get a clear insight of the physical problem, numerical results are displayed with the help of graphical illustrations. We have computed solutions for translational velocity, dimensionless temperature, dimensionless species (mass transfer) function and dimensionless micro-rotation for the following general values: $s = 0.5, P_r = 0.7, (air), S_c = 0.2$ (hydrogen at 25 Celsius and 1 atmosphere pressure, (see Gebhart and Pera [21]) $, G_r = 5, G_m = 5, V_0 = 0.5, R_e = 1, F_s = 0.5, B = 0.01, GG = 1, \lambda = 1$. In the present analysis we have excluded plots (for conservation of space) for the effects of $V_0, R_e, B, GG \, and \, \lambda$, which are fixed in the computations. Figures 2 and 3 illustrate variation of velocity function, temperature function, mass transfer function, micro-rotation function and versus η for various thermophoresis $\kappa = 0,1,5,10,50,70,100$. In figure 2 as κ rises the velocity profiles are increased substantially. The lowest velocity corresponds to the case for no thermophoresis effect i.e. $\kappa = 0$. All profiles then decay monotonically towards zero as $\eta \to \infty$, and the profiles are asymptotically very smooth, indicating that convergence has been achieved comfortably by $\eta \approx 3.5$. A rise in κ causes a distinct fall in the temperature profiles. Higher κ values imply more heat is convicted away from the plate so that temperatures decrease rapidly near the plate surface. All profiles decay asymptotically to zero as $\eta \to \infty$ (11). In figure 3 illustrates the variation of dimensionless concentration function, dimensionless angular velocity versus η . as κ rises the concentration parameters are increased substantially. As noted earlier, at $\eta = 0$, i.e. at the wall (vertical bounding surface), all h profiles have different values since the condition at the wall is defined by $h(0) = -sf''(0)$. Figure 4 illustrates the non-dimensional temperature function distribution with η for various R values. Temperatures decrease markedly as R increases from 0 to 20. Figures 5 and 6, illustrate the influence of the porous hydrodynamical parameters, D_a on the velocity, species concentration fields, and micro-rotation respectively. Figure 5 indicates that

translational velocity profiles clearly increase as D_a rises from 0.1 to 10 . A rise in D_a implies a rise in porous media matrix permeability (k) which corresponds to a reduction in the Darcian drag force, embodied in the following term in the transformed translational momentum equation (10). In all cases, the velocity decays systematically to zero as $\eta \to \infty$. Figure 6 shows that concentrations and micro-rotation fall with rising Da values. All profiles descend gradually from a maximum of 1 at the wall to zero far away from the wall. The graphs show that concentration profiles in Darcy- Forchheimer media may be boosted with less porous materials (lower permeability). This can be exploited in enhancing energy and mass transfer in various specialized applications in industry, where the permeability of a system, unlike geophysical systems, can be varied. Also, depicts the variation of dimensionless angular velocity with η for various D_a values. As noted earlier, at $\eta = 0$ i.e. at the wall (vertical bounding surface), all h profiles have different values since the condition at the wall is defined by $h(0) = -sf''(0)$. $h(0)$ is always non-zero since $s = 0$ and $f''(0) \neq 0$. For D_a up to 0.1, all profiles descend smoothly to zero as $\eta \to \infty$, never crossing. It would appear therefore that larger permeability materials can be used to reduce micro-rotational effects in suspension fluids. Figure 7 shows the influence of Prandtl number on the dimensionless temperature function. A rise in P_r from 0.7 (air) and 1, corresponds to a decrease in thermal conductivity of the fluid (i.e. an increase in Prandtl number for constant values of dynamic viscosity and specific heat capacity. Temperatures are therefore dramatically enhanced throughout the domain i.e. $0 \prec \eta \prec 1$. This is consistent with the well-known behaviour associated with lower thermal conductivity fluids (high Prandtl numbers) compared with higher thermal conductivity fluids (low Prandtl numbers), which is verified by many experiments described in the classical exposition by Schlichting [20]. Figure 8 illustrates the variation of dimensionless concentration function ϕ versus η with various Schmidt numbers (S_c). Smaller S_c values correspond to hydrogen gas as the species diffusing $(S_c = 2.0)$ and larger values to Methanol diffusing in air $(S_c = 1.0)$ and Ethylbenzene in air $(S_c = 2.0)$, as indicated by Gebhart and Pera [21]. Our numerical calculations are executed for $(S_c = 2.0)$ P_r = 0.7, so that $P_r \neq S_c$, and physically this implies that the thermal and species diffusion regions are of different extents. S_c measures the relative effectiveness of momentum and mass transport by diffusion. As S_c is increased, ϕ values consistently decrease, a phenomenon which has been reported in a number of other studies on coupled heat and mass transfer in porous media, as discussed for example by Kim [22].

Figures 9 -12 illustrate variation of velocity function, temperature function, micro-rotation function and mass transfer function versus η for various Grashof numbers G_r and modified Grashof numbers G_m. In figure 9 as G_r rises the velocity profiles are increased substantially. The lowest velocity corresponds to the case for forced convection i.e. $G_r = 0$. In the zone near to the plate surface, peak velocities arise at $\eta \approx 0.5$, for all profiles. On the other hand, a rise in G_r causes a distinct fall in the temperature profiles. Higher G_r values imply more heat is convected away from the plate so that temperatures decrease rapidly near the plate surface (in the range $0.5 \prec \eta \prec 3.5$ approximately). Figure 10 illustrates the variation of

dimensionless concentration function and micro-rotation profiles versus η. Again we notice a strong decrease with increase in G_r values, so that the lowest species concentrations correspond to the highest G_r values i.e. buoyancy reduces concentration values. Monotonic decay of all profiles is observed as $\eta \to \infty$ (8). While no buoyancy term arises in the dimensionless angular momentum equation we note that the strong coupling of the translational velocity fields and micro-rotation fields exists. A micro-rotation terms also occurs in the second function in equation (17), which further serves to couple the angular and translational velocity fields. Buoyancy therefore indirectly, but strongly, affects the micro-rotation profile. We observe that for forced convection ($G_r = 0$) and weaker free convection regimes ($G_r = 5,10$), the micro-rotation profiles are always positive. At η = 0 i.e. at the wall, all profiles have different values as this initial condition is dictated by equation (11) where $h(0) = -sf''(0)$ which is always non-zero since $s = 0.5$ and $f''(0) \neq 0$. Figures 11 and 12 Same behavior like Figs. 9 and 10.

In Figure 13 we observe that as s increases from zero to 1.0, the micro-rotation is increased substantially especially in the region near the wall i.e. $0 \prec \eta \prec 2$ All profiles converge at $\eta = 2$, and descend steadily to zero as $\eta \to \infty$.We note that the parameter s only occurs in the boundary conditions and that it physically relates to the concentration of micro-elements at the wall. We note that this initial boundary condition for micro-rotation corresponds to the vanishing of the anti-symmetric part of the stress tensor and corresponds to weak concentrations of the micro-elements of the micropolar fluid. The particle spin is equal to the fluid vorticity at the boundary for fine particle suspensions. $s = 0$ implies zero spin i.e. the particle stagnate in a rotational sense at the wall. $s = 0.25, 0.5, 1$ implies greater concentrations of micro-elements respectively. Clearly we see that greater s values imply greater micro-rotation, as reflected in our graph.

Conclusions

A mathematical model has been presented for the viscous, incompressible heat and mass transfer of a micropolar fluid through a non-Darcian porous medium with buoyancy, Thermophoresis and radiation effects, viscous heating and wall transpiration present. The model has been transformed and rendered into dimensionless form. Our numerical results indicate that generally:

-a) Increasing κ increases the dimensionless translational velocities (f' and mass transfer function (ϕ), but decreases temperature function (θ) and angular velocity (h).

-b) Increasing R increases the dimensionless temperature function (θ).

-c) Increasing D_a increases dimensionless translational velocities (f'), but decreases mass transfer function (ϕ) and angular velocity (h).

-d) Increasing P_r decreases the dimensionless temperature function (θ).

-f) Increasing S_c decreases dimensionless mass transfer function (ϕ) values.

-g) Increasing G_r *and* G_m (buoyancy parameter) increases dimensionless translational velocity (f'), but decreases temperature function (θ), mass transfer function (ϕ) and angular velocity (h) (micro-rotation).

-h) Increasing s increases the dimensionless micro-rotation (h)

The model presented has applications in plastic processing technologies and is currently being extended to incorporate the effects thermal stratification of the porous medium, an important feature in geophysical systems.

References

[1] Eringen, A. C., Simple Microfluids, Int. J. Engineering Science, (1964),2, 205-217.

[2] Ramachandran, P.S. and Mathur, M.N., Heat transfer in boundary layer flow of a micropolar fluid past a curved surface with suction and injection, Int. J. Engineering Science, (1964), 17, 625-639.

[3] Vidyanidhi,V. and Sreeramachandra Murty,M., The dispersion of a chemically-reacting solute in a micropolar fluid, Int. J. Engineering Science, (1976),14, 1127-1133.

[4] Soundalgekar, V.M. and Takhar, H.S., Heat transfer in wedge flow of a micropolar fluid. Proceedings 8th International Conference on Rheology, Naples, Italy, (1980)321-325.

[5] N. P. Migun and P. P. Prokhorenko, Heating of a micropolar liquid due to viscous energy dissipation in channels. II. Couette flow, J. Engineering Physics and Thermophysics, (1984)46, 3 , 278 – 282.

[6] M. M. Khonsari and D. E. Brewe , Effect of viscous dissipation on the lubrication characteristics of micropolar fluids, Acta Mechanica, 1/4 (1994).

[7] I. A. Hassanien, A. Y. Bakier, R. S. R. Gorla, Natural convection boundary layer flow of a micropolar fluid, ZAMMZ. angew. Math. Mech. 77(1997)10, 751-755.

[8] I.A. Hassanien , T.H. Al-arabi "Non-Darcy unsteady mixed convection flow near the stagnation point on a heated vertical surface embedded in a porous medium with thermal radiation and variable viscosity" Commun Nonlinear Sci Numer Simulat (2008) (in press)

[9] Ching-Yang Cheng Natural convection heat and mass transfer from a sphere in micropolar fluids with constant wall temperature and concentration International Communications in Heat and Mass Transfer xx (2008) (in press)

[10] R. Nazar, N. Amin, T. Grosan, I. Pop, Free convection boundary layer on an isothermal sphere in a micropolar fluid, International Communications in Heat and Mass Transfer 29 (2002) 377–386.

[11] M. K. Partha Thermophoresis particle deposition in free convection on a vertical plate embedded in a fluid saturated non-Darcy porous medium is studied using similarity solution technique Heat Mass Transfer (2008) 44:969–977

[12] Ingham, D. B. and Pop, I. (Editors), Transport Phenomena in Porous Media: Volume 2. Pergamon Press, Oxford (2002).

[13] Vafai, K. and Tien, C.L., Boundary and Inertia Effects on Flow and Heat Transfer in Porous Media, Int. J. Heat Mass Transfer, (1981),24, 195-203.

[14] O. A. Bég, Prasad, H.S. Takhar, V. M. Soundalgekar, Thermal convective flow in an isotropic, homogenous medium using Brinkman's vorticity diffusion model: Numerical Study, Int. J. Numerical Methods in Heat and Fluid Flow, (1998),8, 59-89.

[15]O. A. Bég , J. Zueco , H.S. Takhar, Laminar free convection from a continuously-moving vertical surface in thermally-stratified non-Darcian high-porosity medium: Network numerical

study, I. C. Heat and Mass Transfer, (2008),in press.

[16] H. S. Takhar, R. Bhargavaa , S. Rawat, Tasveer A. Bég, O. Anwar Bégd, Hung,Tin-Kan "Biomagnetic hydrodynamics in a 2-dimensional non-Darcian porous medium: finite element study" , Journal of theoretical and applied mechanics, 2007, vol, 37, no. 2, pp. 59-76.

[17] Chamkha, A. J., Pop, I., Effect of Thermophoresis Particle Deposition in Free Convection Boundary Layer from a Vertical Flat Plate Embedded in a Porous Medium, *Inter. Comm.Heat Mass Transfer, 31* (2004), pp. 421-430.

[18] A. Y. Bakier and M. A. Mansour " Combined of magnetic field and thermophoresis particle deposition in free convection boundary layer from a vertical flat plate embedded in a porous medium" J. Thermal Science: Vol. 11 (2007), No. 1, pp. 65-74.

[19] M.Q. Brewster, Thermal Radiative Transfer Properties, Wiley, Canada, 1992.

[20] Schlichting, H., Boundary-Layer Theory, McGraw-Hill, New York , 7th Edn (1979).

[21] Gebhart, B. and Pera, L., Int. J. Heat and Mass Transfer, 14, 2025 (1971).

[22] Kim, Y.J., Heat and mass transfer in MHD micropolar flow over a vertical moving porous plate in a porous medium, Transp. Porous Media J., 56, 17-37 (2004).

Nomenclature

C species concentration in the boundary layer...

C_∞ Species concentration of the ambient fluid

C_p specific heat due to constant pressure

D chemical molecular diffusivity

f dimensionless stream function

g acceleration due to gravity

h dimensionless microrotation component

N micropolar of the fluid in the boundary layer

κ thermophoretic coefficient

P_r Prandtl number

S_c Schmidt number

T temperature of the fluid in the boundary layer

T_∞ temperature of the ambient fluid

T_w temperature at the surface

$V(x)$ transpiration velocity

u, v, the x- and y-components of the velocity field..

U_0 velocity at the wall (vertical surface)

s the surface parameter

V_T thermophoretic velocity

x, y axis in direction along and normal to the plate.....

Greek symbols

α thermal diffusivity……

β volumetric expansion coefficient of temperature

ρ is micropolar fluid density

ψ stream function.....

γ spin-gradient viscosity

η non-dimensional pseudo-similarity variable

ν kinematic coefficient of viscosity .

λ fluid viscosity. .....

θ dimensionless temperature function

φ dimensionless species concentration

Figure 1: Physical Model and Coordinate System

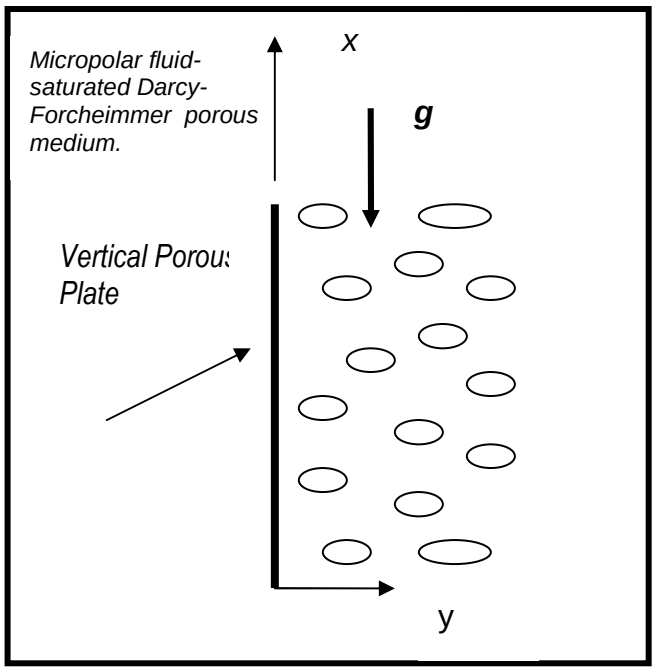

Fig 2: f' and θ versus η for various κ values

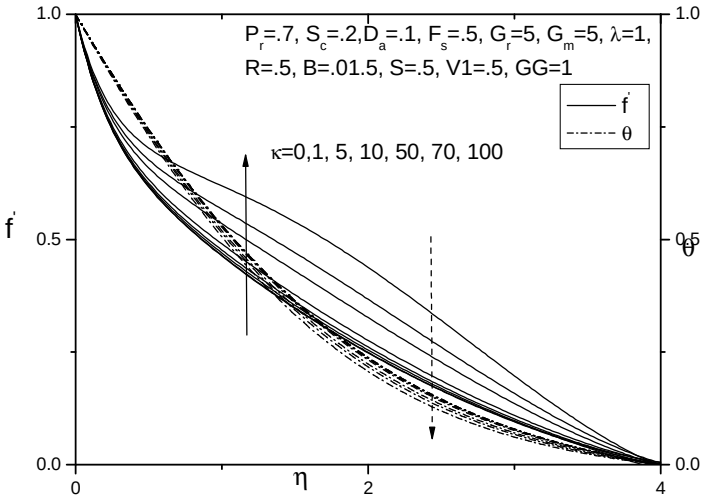

Fig 3: ϕ and h versus η for various κ values

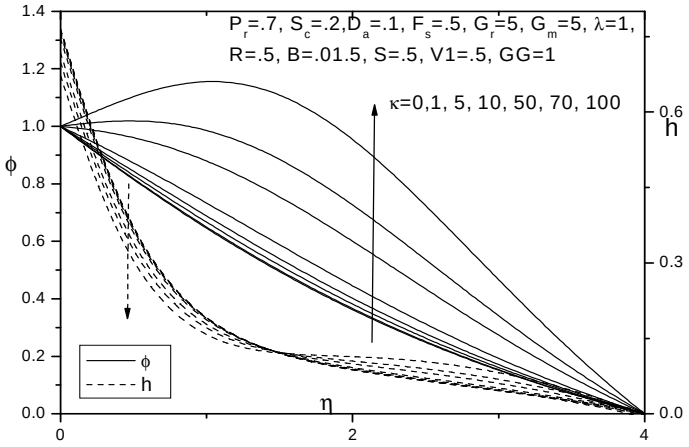

Fig 4: θ versus η for various R values

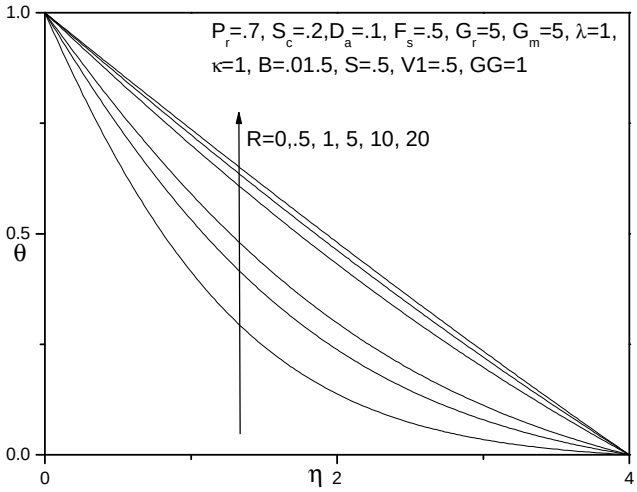

Fig 5: f' versus η for various D_a values

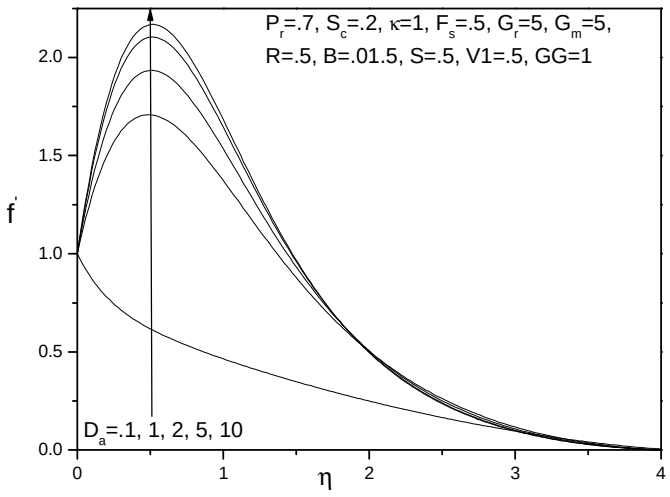

Fig 6: ϕ and h versus η for various D_a values

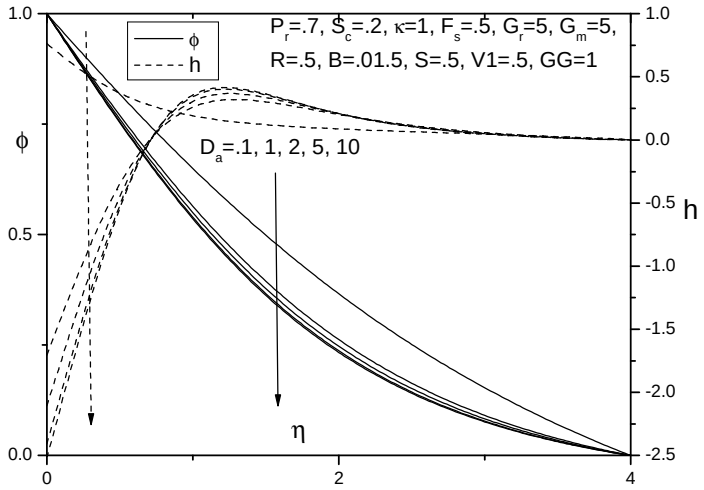

Fig 7: θ versus η for various P_r values

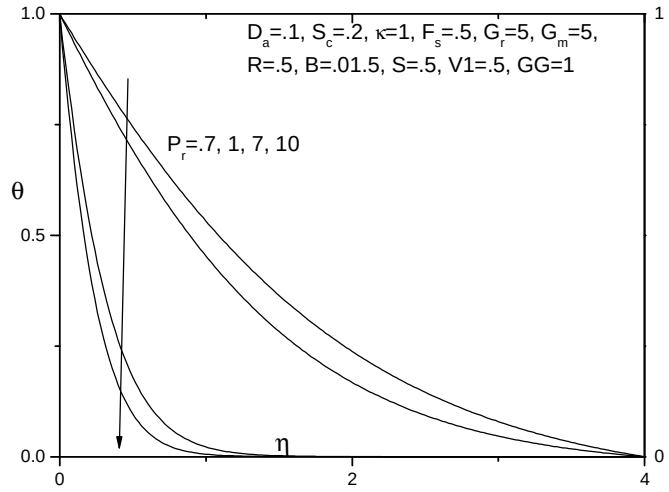

Fig 8: ϕ versus η for various S_c values

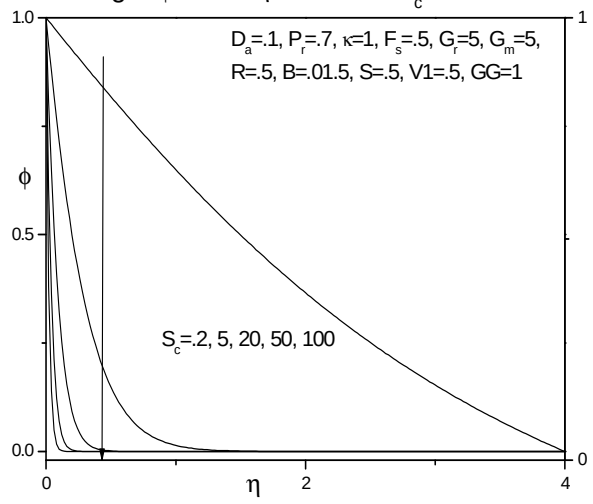

Fig 9: f' and θ versus η for various G_r values

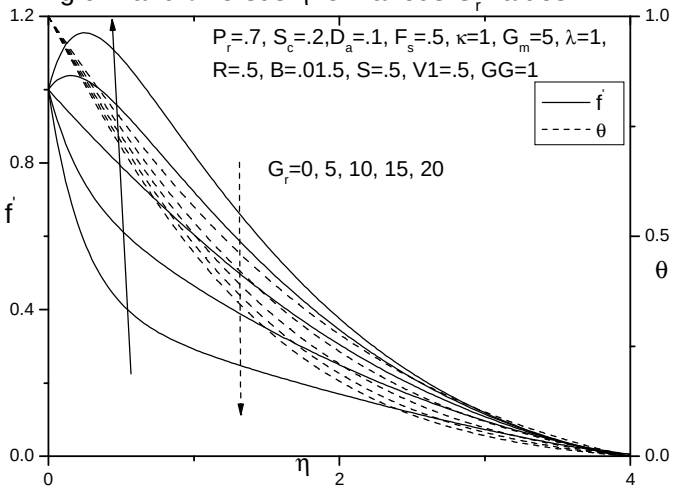

Fig 10: ϕ and h versus η for various G_r values

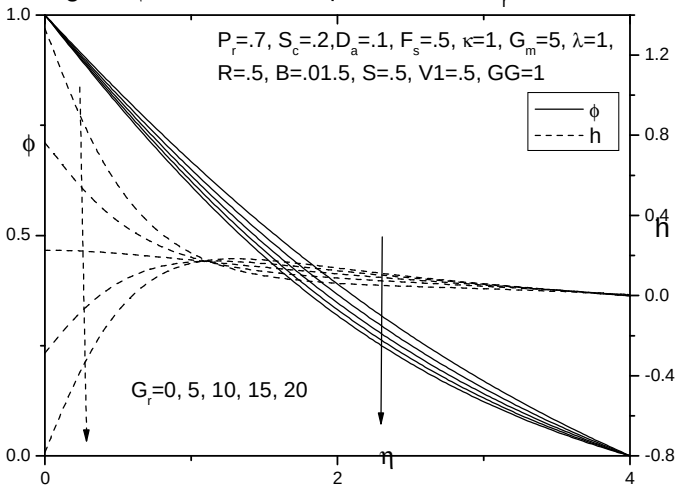

Fig 11: f' and θ versus η for various G_m values

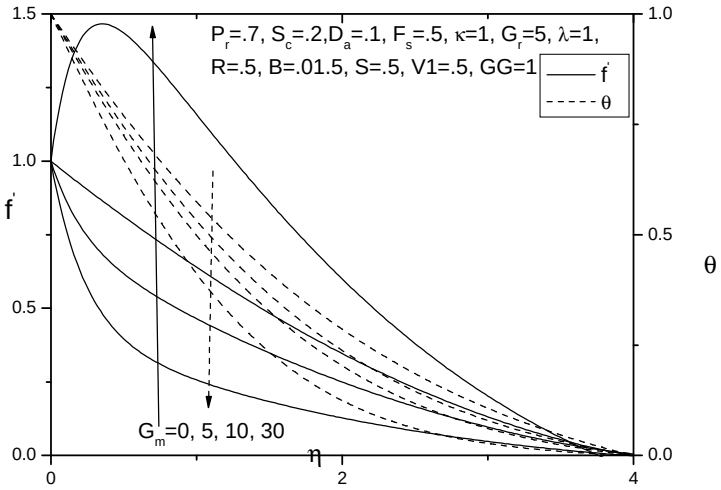

Fig 12: ϕ and h versus η for various G_m values

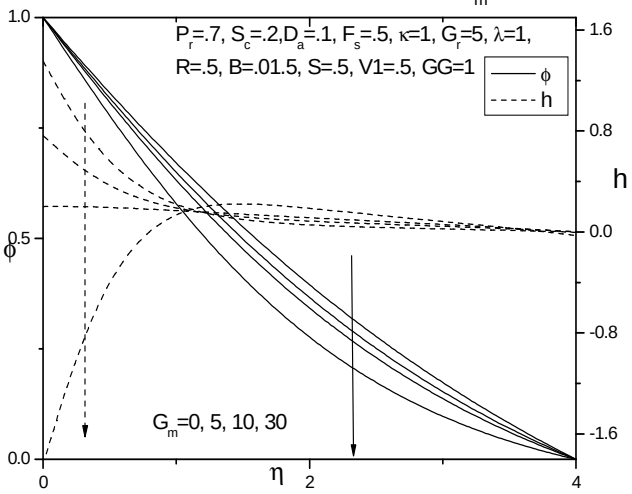

Fig 13: h versus η for various S_c values